AIP Journal of Applied Physics

Improvement in plasma illumination properties of ultrananocrystalline diamond films by grain boundary engineering

K. J. Sankaran, K. Srinivasu, H. C. Chen, C. L. Dong, K. C. Leou, C. Y. Lee, N. H. Tai, and I. N. Lin

Citation: Journal of Applied Physics **114**, 054304 (2013); doi: 10.1063/1.4817377
View online: http://dx.doi.org/10.1063/1.4817377
View Table of Contents: http://scitation.aip.org/content/aip/journal/jap/114/5?ver=pdfcov
Published by the AIP Publishing

Articles you may be interested in

Origin of graphitic filaments on improving the electron field emission properties of negative bias-enhanced grown ultrananocrystalline diamond films in CH4/Ar plasma
J. Appl. Phys. **116**, 163102 (2014); 10.1063/1.4899245

Direct observation and mechanism for enhanced field emission sites in platinum ion implanted/post-annealed ultrananocrystalline diamond films
Appl. Phys. Lett. **105**, 163109 (2014); 10.1063/1.4898571

Enhancing electrical conductivity and electron field emission properties of ultrananocrystalline diamond films by copper ion implantation and annealing
J. Appl. Phys. **115**, 063701 (2014); 10.1063/1.4865325

Gold ion implantation induced high conductivity and enhanced electron field emission properties in ultrananocrystalline diamond films
Appl. Phys. Lett. **102**, 061604 (2013); 10.1063/1.4792744

Fabrication of free-standing highly conducting ultrananocrystalline diamond films with enhanced electron field emission properties
Appl. Phys. Lett. **101**, 241604 (2012); 10.1063/1.4770513

[This article is copyrighted as indicated in the article. Reuse of AIP content is subject to the terms at: http://scitation.aip.org/termsconditions. Downloaded to] IP: 163.13.36.187 On: Mon, 27 Oct 2014 02:41:45

JOURNAL OF APPLIED PHYSICS 114, 054304 (2013)

Improvement in plasma illumination properties of ultrananocrystalline diamond films by grain boundary engineering

K. J. Sankaran,[1] K. Srinivasu,[2] H. C. Chen,[3] C. L. Dong,[4] K. C. Leou,[2] C. Y. Lee,[1]
N. H. Tai,[1,a)] and I. N. Lin[3,b)]
[1]Department of Materials Science and Engineering, National Tsing Hua University, Hsinchu 300, Taiwan
[2]Department of Engineering and System Science, National Tsing Hua University, Hsinchu 300, Taiwan
[3]Department of Physics, Tamkang University, Tamsui 251, Taiwan
[4]Scientific Research Division, National Synchrotron Radiation Research Center, Hsinchu 300, Taiwan

(Received 9 May 2013; accepted 18 July 2013; published online 2 August 2013)

Microstructural evolution of ultrananocrystalline diamond (UNCD) films as a function of substrate temperature (T_S) and/or by introducing H_2 in Ar/CH_4 plasma is investigated. Variation of the sp^2 and sp^3 carbon content is analyzed using UV-Raman and near-edge X-ray absorption fine structure spectra. Morphological and microstructural studies confirm that films deposited using Ar/CH_4 plasma at low T_S consist of a random distribution of spherically shaped ultra-nano diamond grains with distinct sp^2-bonded grain boundaries, which are attributed to the adherence of CH radicals to the nano-sized diamond clusters. By increasing T_S, adhering efficiency of CH radicals to the diamond lattice drops and *trans*-polyacetylene (*t*-PA) encapsulating the nano-sized diamond grains break, whereas the addition of 1.5% H_2 in Ar/CH_4 plasma at low T_S induces atomic hydrogen that preferentially etches out the *t*-PA attached to ultra-nano diamond grains. Both cases make the sp^3-diamond phase less passivated. This leads to C_2 radicals attaching to the diamond lattice promoting elongated clustered grains along with a complicated defect structure. Such a grain growth model is highly correlated to explain the technologically important functional property, namely, plasma illumination (PI) of UNCD films. Superior PI properties, viz. low threshold field of 0.21 V/μm with a high PI current density of 4.10 mA/cm^2 (at an applied field of 0.25 V/μm) and high γ-coefficient (0.2604) are observed for the UNCD films possessing ultra-nano grains with a large fraction of grain boundary phases. The grain boundary component consists of a large amount of sp^2-carbon phases that possibly form interconnected paths for facilitating the transport of electrons and the electron field emission process that markedly enhance PI properties.
© 2013 AIP Publishing LLC. [http://dx.doi.org/10.1063/1.4817377]

I. INTRODUCTION

Microplasma science and technology, a new photonics technology, is a juncture of plasma science, optoelectronics and materials science that offers not only a hierarchy of plasma phenomenology but also device functionality.[1–4] These plasma-based devices reveal great potential for a broad spectrum of applications in microdisplays, material synthesis, and elemental analysis.[5–11] Even though plasma display technology has advanced considerably in the past decade, the luminous efficiency of the plasma devices is still inadequate. The development of a cathode material to emit ion-induced secondary electrons for improving the performance of plasma illumination (PI) devices is still ongoing. MgO is typically used as a coating in plasma cells as it possesses a large ion-induced secondary electron emission (SEE) coefficient, or γ-coefficient.[12] Diamond usually exhibits a large γ-coefficient owing to diamond's wide band gap (5.5 eV) and negative electron affinity (NEA).[13] The Paschen-curve based γ-measurement[14] indicates that diamond films synthesized via chemical vapor deposition possess a higher γ-coefficient than that of single crystal MgO. Diamond is predominantly interesting because of its NEA, low sputtering yield, and insensitivity to various processing conditions. Moreover, the observations by Chakrabarti *et al.*[15] imply that the high γ-coefficient is correlated to the better electron field emission (EFE) properties of the material. As a consequence, high EFE diamond material is being explored for the development of a high γ-coefficient diamond material with enhanced PI characteristics.

Ultrananocrystalline diamond (UNCD) is a special form of diamond that has recently gained a great deal of attention from researchers because of its better EFE properties, along with its ultra-small grain size (5–10 nm) and very smooth surface characteristics. These grains abruptly terminate at wide angle sp^2-bonded grain boundaries.[16] Microstructure of UNCD films is extremely sensitive to film deposition parameters, such as reactant gas ratio, plasma content, and substrate temperature (T_S).[17–20] Appropriate modification and control of microstructures of UNCD films can tailor their physical and chemical properties for developing new applications and technologies. Nano-sizing of diamond crystal will consequently increase the grain boundaries containing non-diamond carbons in the UNCD films, besides appreciably varying the surface characteristics of the films.[21,22] Prior studies have been reported that a proper increase in amorphous carbon (*a-C*) phase grain boundaries and

a)Electronic mail: nhtai@mx.nthu.edu.tw
b)Electronic mail: inanlin@mail.tku.edu.tw

 © 2013 AIP Publishing LLC

[This article is copyrighted as indicated in the article. Reuse of AIP content is subject to the terms at: http://scitation.aip.org/termsconditions. Downloaded to] IP: 163.13.36.187 On: Mon, 27 Oct 2014 02:41:45

formation of nanographites in UNCD films would form the possibly interconnected paths for facilitating the transport of electrons and markedly enhance EFE properties.[23,24] However, the control of the processing parameters on the formation of unique microstructures of ultra-nano diamond grains along with sp^2-bonded grain boundaries is not understood and the mechanism by which the distinctive granular structure influences EFE and PI properties has not been studied.

In this study, a possible mechanism for the enhancement of EFE and PI properties of UNCD films grown using plasma gas mixtures of Ar/CH_4 and Ar/1.5% H_2/CH_4 at various T_S (550–750 °C) are investigated. Field emission scanning electron microscopy (FESEM), UV-Raman spectroscopy, near edge X-ray absorption fine structure (NEXAFS), and transmission electron microscopy (TEM) studies express how the T_S and addition of 1.5% H_2 to the Ar/CH_4 plasma influence the microstructural evolution and variation in the sp^3 and sp^2 carbon phases in the films. Based on these studies, a grain growth model is proposed to describe the EFE and PI properties of UNCD films.

II. EXPERIMENTAL SECTION

Two series of UNCD films were grown on mirror polished Si substrates using a microwave plasma enhanced chemical vapor deposition (MPECVD) system (2.45 GHz 6″ IPLAS-CYRANNUS-I, Troisdorf, Germany). Prior to the deposition of UNCD films, the silicon substrates were preseeded by ultrasonication in methanol solution, containing nano diamond (∼5 nm in diameter) and Ti powders (∼325 mesh), for 45 min to create nucleation sites for growing UNCD films. For the first series of UNCD films, we used Ar (99%)/CH_4 (1%) as the reactant gases with a microwave power of 1200 W and a pressure of 120 Torr (16 kPa). The films were grown at a T_S ranging from 550 to 750 °C. The T_S was kept constant using a heater attached below the substrate holder and the T_S was measured with a thermocouple fixed with the heater. The corresponding films were designated as $UNCD_{nAr}$, where n is the T_S. For the second series, 1.5% H_2 was added to the Ar/CH_4 plasma (Ar/H_2/CH_4 = 97.5/1.5/1) and the films were grown at 1200 W and 110 Torr (14.6 kPa). The T_S was varied from 550 to 750 °C and the corresponding films were designated as $UNCD_{nH}$, where n is the T_S. The two series of films were grown for 60 min and the flow rate of the gases was maintained at 100 sccm.

The morphology and microstructure of the UNCD films were studied using FESEM (JEOL 6500) and TEM (JEOL 2100 F). The bonding characteristics of the films were examined using UV-Raman spectroscopy (λ: 325.0 nm, Renishaw) and NEXAFS spectroscopy. The plasma species were analyzed during the film's deposition process using *in situ* optical emission spectroscopy (OES, BWTEK). The EFE properties of the diamond films were measured with a tunable parallel plate setup, in which the cathode-to-anode distance was controlled using a micrometer. The current-voltage (*I-V*) characteristics were measured using an electrometer (Keithley 237) under pressure below 10^{-6} Torr (1.3×10^{-4} Pa). The EFE parameters were extracted from the obtained *I-V* curves by using the Fowler-Nordheim (F-N) model:[25]

$$J_{EFE} = \left(\frac{A\beta^2E^2}{\varphi}\right)\exp\left(-\frac{B\text{Ø}^{\frac{3}{2}}}{\beta E}\right), \quad (1)$$

where $A = 1.54 \times 10^{-6}$ A eV/V^2 and $B = 6.83 \times 10^9$ eV$^{-3/2}$ V/m, β is the field-enhancement factor, E is the applied field, and φ is the work function of the emitting materials. The point of interception of the straight lines extrapolated from the low and high-field segments of the F-N plots, namely, log (J_{EFE}/E^2) vs. $1/E$, is designated as the turn-on field (E_0), where J_{EFE} is the EFE current density.

The PI characteristics of a microcavity were also investigated, in which an indium tin oxide (ITO)-coated glass was used as anode and the UNCD films were used as cathode. The cathode-to-anode separation was fixed by a polytetrafluoroethylene (PTFE) spacer (1.0 mm in thickness). A circular hole about 8.0 mm in diameter was cut out from the (PTFE) spacer to form a microcavity. The plasma was triggered using a pulsed direct current voltage in a bipolar pulse mode (20 ms square pulse, 6 kHz repetition rate). Prior to measurements, all samples were heated at 200 °C for 1 h to remove moisture from the surface of the films. The chamber was evacuated to reach a base pressure of 0.1 mTorr (13 MPa) and then purged with Ar for 10 min. The Ar gas was channeled into the chamber at a flow rate of 10 sccm throughout the measurements. The plasma current vs. applied voltage was measured using an electrometer (Keithley 237). The same configuration was used to evaluate the γ-coefficient of the films. From this measurement, at a fixed distance of d = 1.0 mm between the two electrodes and with Ar pressure (p) varied from 0.1 to 8.0 Torr (13.3–1066.5 Pa), the breakdown voltages for each value of "pd" were measured and Paschen curves were obtained.

In general, for every gas, there will be high breakdown voltages either at low pressures called vacuum breakdown or at high pressures called high pressure insulation,[26] viz. there is an optimum "pd" for the lowest breakdown voltages. Mariotti *et al.*[27] explained the way of estimating the γ value from the lowest breakdown voltage $(V_{bk})_{min}$ of a Paschen curve, using the relationship

$$\gamma = \frac{1}{\exp\left(Apd.\exp\left(\frac{-Bpd}{V}\right)\right) - 1}, \quad (2)$$

where $A = 0.09$ Pa^{-1} cm^{-1} and $B = 1.35$ V Pa^{-1} cm^{-1} for Ar gas and V was the applied voltage.

III. RESULTS AND DISCUSSION

Figure 1 shows the FESEM images of the densely packed UNCD films grown in Ar/CH_4 and Ar/1.5% H_2/CH_4 plasmas at various T_S in the same MPECVD system. From the FESEM images, we observe the apparent changes in the morphology of the films with the change in T_S and the reactant gas content. The morphology of the $UNCD_{550Ar}$ shows random and spherically structured grains in the films

[This article is copyrighted as indicated in the article. Reuse of AIP content is subject to the terms at: http://scitation.aip.org/termsconditions. Downloaded to] IP: 163.13.36.187 On: Mon, 27 Oct 2014 02:41:45

(Fig. 1(a)), while that for $UNCD_{650Ar}$ and $UNCD_{750Ar}$ show the elongated grains (Figs. 1(b) and 1(c), respectively), indicating the occurrence of lateral growth of grains. The morphology of the $UNCD_{550H}$ films also shows elongated grains (Fig. 1(d)), which is comparable with that of $UNCD_{750Ar}$ films. Such an observation implies that the addition of 1.5% H_2 in Ar/CH_4 plasma has the same effect as increasing the T_S on the modification of granular structure in UNCD films. The grains of the $UNCD_{650H}$ and $UNCD_{750H}$ (Figs. 1(e) and 1(f), respectively) are much larger in size compared with that of $UNCD_{550H}$, which is an indication of greater lateral dimensional growth of grains.

Raman spectroscopy is an important technique to explore the bonding character of different carbon phases present in UNCD films. Figures 2(a) and 2(b) depict the UV-Raman spectra of samples deposited in Ar/CH_4 and Ar/1.5% H_2/CH_4 plasma at different T_S The advantage of UV-Raman spectroscopy (325 nm) is that it is more sensitive to the sp^3-bonded carbon phases in the films and can also decrease any photoluminescence background present in the visible-Raman spectra (632.8 nm), enabling a much better signal to noise ratio and hence attainability of clear spectra.[28,29] Apart from the diffused peaks at $\sim$1140 cm^{-1} (ν-band), $\sim$1360 cm^{-1} (D-band), and $\sim$1540 cm^{-1} (G-band), a sharp peak at $\sim$1330 cm^{-1} is also observed in these spectra, revealing the first-order diamond phase in the films.[30,31] The diffused peaks represent the existence of a *trans*-polyacetylene (*t*-PA) phase along the grain boundaries. Figures 2(c) and 2(d) present the variation of $I_{t\text{-PA}}/I_{diamond}$ and $I_{diamond}/(I_D+I_G)$ ratios of the two series of films under different T_S. In both UNCD films, the $I_{t\text{-PA}}/I_{diamond}$ ratio shows a decrease with increase in T_S, signaling the relative decrease in the *t*-PA phase. Whereas an increase in the diamond phase with respect to the sp^2 carbon phase in the films is observed from the increasing trend of the $I_{diamond}/(I_D+I_G)$ ratio with T_S. In these studies, it is observed that for $T_S > 650\,^\circ$C the change in the two plots is insignificant, confirming that the higher T_S value can bring about a change in the structure and distribution of the sp^2 as well as sp^3 phases in the films.

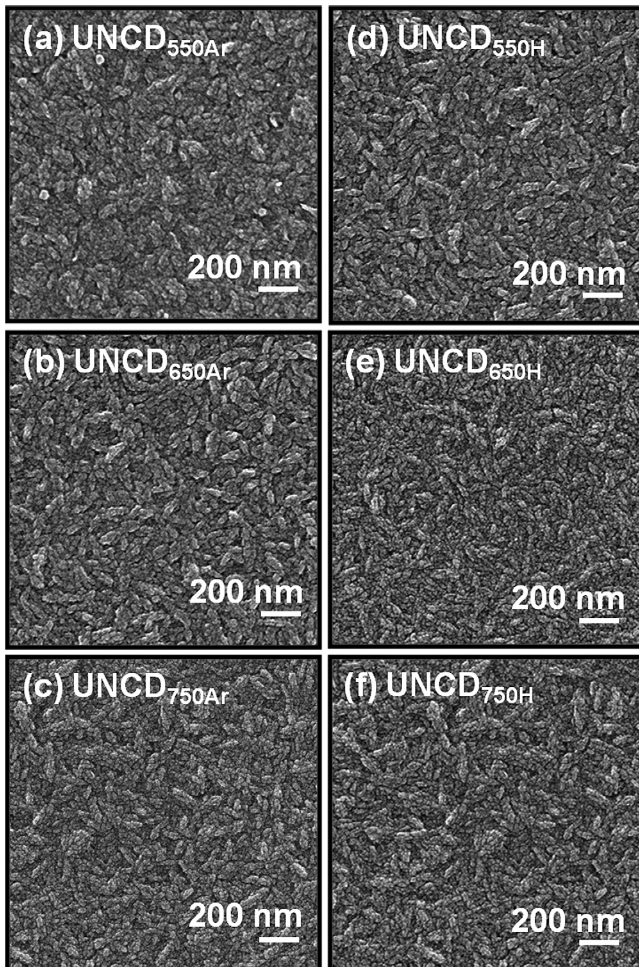

FIG. 1. FESEM images of (a) $UNCD_{550Ar}$, (b) $UNCD_{650Ar}$, (c) $UNCD_{750Ar}$, (d) $UNCD_{550H}$, (e) $UNCD_{650H}$, and (f) $UNCD_{750H}$.

For the purpose of more explicitly differentiating the various types of carbon bonding configuration in the films, NEXAFS spectroscopy was used. Figures 3(a) and 3(b) show the NEXAFS spectra of the UNCD films deposited in the Ar/CH_4 and Ar/1.5% H_2/CH_4 plasma, respectively, at different T_S, clearly ascertaining that the major configuration of carbon is the sp^3 diamond phase with a smaller amount of sp^2 phase distributed in the films.[32] A sharp peak at $\sim$289.0 eV corresponds to the diamond electron core excitation of C-C (1 s)-σ^*, while the sp^3 diamond phase and a weak dip observed at 302.0 eV is assigned to the second absorption band gap of diamond.[33–35] The small peak at $\sim$283.5 eV is assigned to the C1s-π^* transition corresponding to the sp^2 phase.[36,37] Moreover, a weak bump at 286.7 eV observed between the π^* and σ^* bonds is attributed to the C-H bond,[38] which originates from the absorption of hydrocarbon at grain boundaries during the film deposition process.[39] Figure 3(c) shows the sp^2/sp^3 ratio, which is the ratio of integral intensity of C1s-π^* and C-C (1 s)-σ^* peaks, for both $UNCD_{nAr}$ and $UNCD_{nH}$ films. This figure shows that the addition of H_2 in Ar/CH_4 plasma is more effective in reducing the sp^2 phase located along the grain boundaries for the UNCD films than the increase in T_S. The $UNCD_{550Ar}$ films contain larger amount of sp^2 and C-H phases as compared with the other UNCD films.

Figures 4(a) and 4(b) show the EFE properties of the films deposited in Ar/CH_4 and Ar/1.5% H_2/CH_4 plasma, respectively, which are plotted as the EFE current density vs. applied field (J_{EFE}-E) with the corresponding F-N plots in the insets. The EFE parameters, E_0 and J_{EFE}, are extracted from these plots and are listed in Table I. For both plasma conditions, E_0 increases with T_S (solid curves, Fig. 4(c)). For UNCD films grown using Ar/CH_4 plasma, the J_{EFE} at 50.0 V/μm decreases monotonously with T_S from $(J_{EFE})_{550Ar} \geq 2.71$ mA/cm^2 to $(J_{EFE})_{750Ar} \leq 1.3$ mA/cm^2 (dashed curve I, Fig. 4(c)). The same tendency is observed for the films grown in Ar/1.5% H_2/CH_4 plasma (dashed curve II, Fig. 4(c)), i.e., the EFE $(J_{EFE})_{550H} \geq 1.61$ mA/cm^2 and $(J_{EFE})_{750H} \leq 0.31$ mA/cm^2 at 65.0 V/μm. The UNCD films grown in Ar/CH_4 plasma show better EFE behavior than those grown in Ar/1.5% H_2/CH_4 plasma, i.e., the lower E_0 and higher J_{EFE}, and the $UNCD_{550Ar}$ films show the best EFE behavior among all other UNCD films.

[This article is copyrighted as indicated in the article. Reuse of AIP content is subject to the terms at: http://scitation.aip.org/termsconditions. Downloaded to] IP: 163.13.36.187 On: Mon, 27 Oct 2014 02:41:45

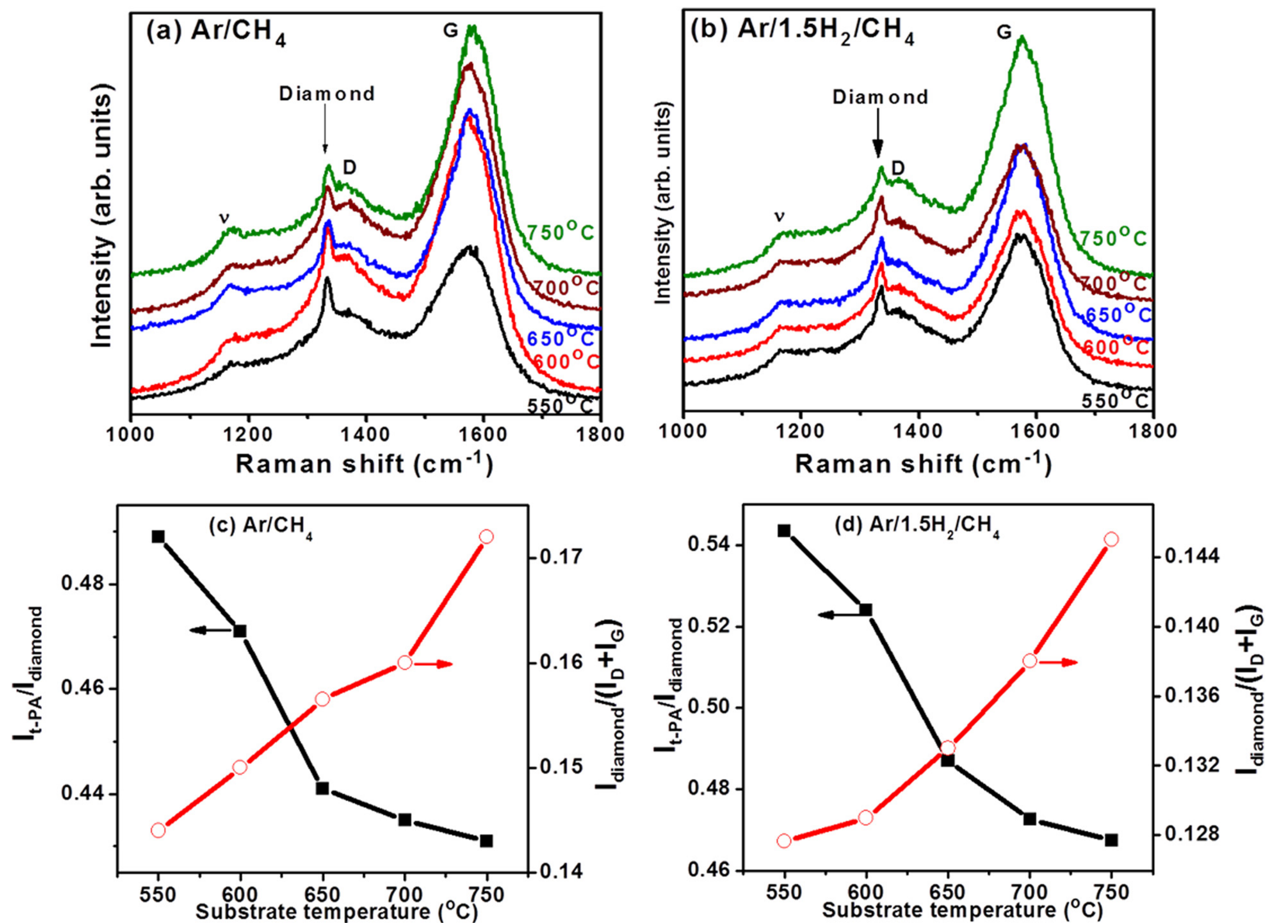

FIG. 2. T_S dependence of UV-Raman spectra of UNCD films deposited in (a) Ar/CH_4 plasma and (b) Ar/1.5% H_2/CH_4 plasma. $I_{t\text{-}PA}/(I_{diamond})$ and $I_{diamond}/(I_{D+}I_G)$ of UNCD films deposited in (c) Ar/CH_4 plasma and (d) Ar/1.5% H_2/CH_4 plasma, where $I_{t\text{-}PA}$, I_D, and I_G are the integrated intensities of the ν, D-band, and G-band peaks, respectively.

On the other hand, Fig. 5 shows the series of photographs of the PI behavior of the plasma devices, which utilized the UNCD films grown in Ar/CH_4 and Ar/1.5%H_2/CH_4 at various T_S as cathode materials. This figure shows that the devices using $UNCD_{550Ar}$ films as cathodes (Fig. 5(a)) exhibit superior illumination behavior to those using $UNCD_{750Ar}$, $UNCD_{550H}$, and $UNCD_{750H}$ as cathodes (Figs. 5(b), 5(c), and 5(d), respectively). The threshold field (E_{th}) for inducing the PI process varies only moderately with T_S and is slightly larger for devices using $UNCD_{nH}$ films as the cathode. The E_{th} is lowest for the $UNCD_{550Ar}$-cathoded devices. However, J_{PI} varies markedly when using a different kind of UNCD as cathodes. The PI characteristics of the plasma devices are better illustrated by the variation of the plasma current density (J_{PI}) versus E, which is plotted in Figs. 6(a) and 6(b). For both series of UNCD films, as T_S increases the E_{th} increases, while J_{PI} decreases. The trend is similar with the change in EFE behavior (cf. Fig. 4). The values of E_{th} and J_{PI} are extracted from these figures and are listed in Table II. For UNCD films grown using Ar/CH_4 plasma, the J_{PI} at 0.25 V/μm decreases monotonously from $(J_{PI})_{550Ar} = 4.38\,mA/cm^2$ to $(J_{PI})_{750Ar} = 2.54\,mA/cm^2$ (Fig. 6(a)). The same trend is observed for the films grown in Ar/1.5% H_2/CH_4 plasma, i.e., the $(J_{PI})_{550H} = 2.54\,mA/cm^2$ and $(J_{PI})_{750H} = 1.41\,mA/cm^2$ at 0.25 V/μm (Fig. 6(b)). Restated, the lowest E_{th} value of 0.21 V/μm and the largest J_{PI} of 6.5 mA/cm^2 at 0.25 V/μm applied field are observed for the $UNCD_{550Ar}$ films (curve I, Fig. 6(a)).

The above observations indicate that microplasma devices perform better when the cathode materials possess superior EFE properties. However, there is a subtle difference in the material's dependence of the EFE and PI behavior. The E_0 for the EFE process increases markedly as T_S increases or as 1.5% H_2 is added in Ar/CH_4 plasma, whereas the E_{th} for igniting the plasma only changes moderately (cf. Tables I and II). Nevertheless, the cathode materials with higher J_{EFE} do significantly enhance the PI process, leading to a larger J_{PI}, viz. $J_{EFE} \sim 2.71\,mA/cm^2$ (at 50.0 V/μm applied field) and $J_{PI} = 4.38\,mA/cm^2$ (at 0.25 V/μm applied field) for $UNCD_{550Ar}$ films. To understand the correlation between the EFE and PI behavior, the SEE properties (γ-coefficient) of these materials were examined.

In general, the γ value can be evaluated by measuring the material's electron current while bombarding it with high energy ions.[12] However, such a measurement is rather difficult. Another way of measuring γ is by analyzing the discharge parameters of the plasma, which were created in between the two parallel electrodes. For the former, the Paschen curves are measured, plotting the breakdown voltage (V_{bk}) of the plasma against the "pd" value, where p is

[This article is copyrighted as indicated in the article. Reuse of AIP content is subject to the terms at: http://scitation.aip.org/termsconditions. Downloaded to] IP: 163.13.36.187 On: Mon, 27 Oct 2014 02:41:45

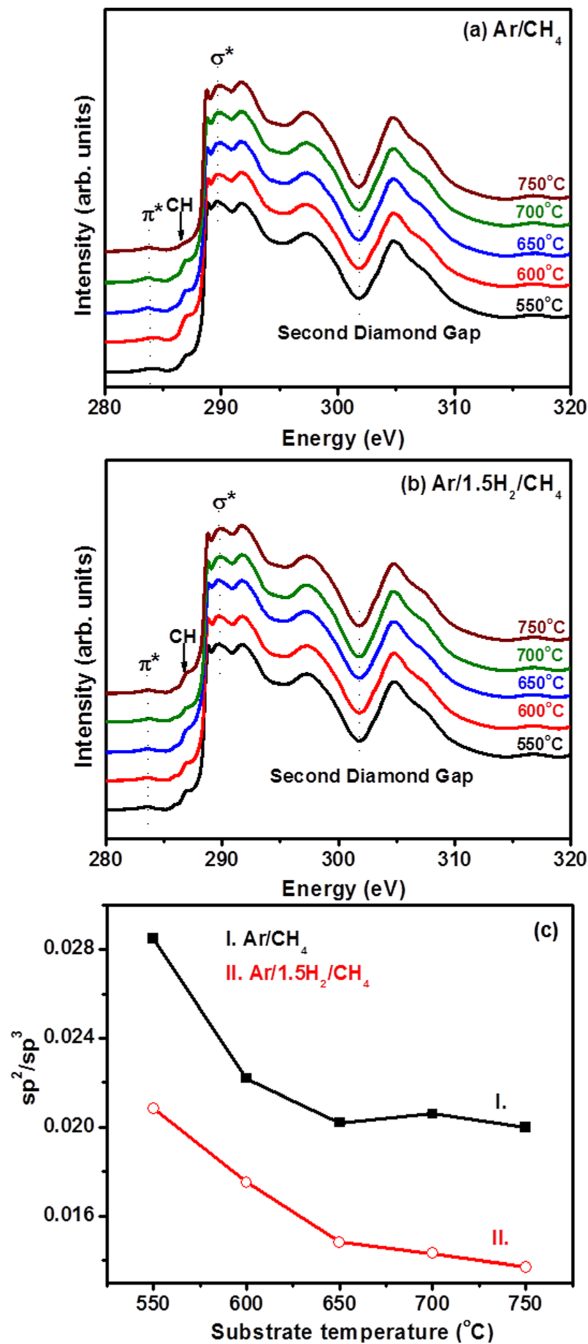

FIG. 3. T_S dependence of NEXAFS spectra of UNCD films deposited in (a) Ar/CH_4 plasma and (b) $Ar/1.5\%\ H_2/CH_4$ plasma; (c) the sp^2/sp^3 ratio of the corresponding UNCD films.

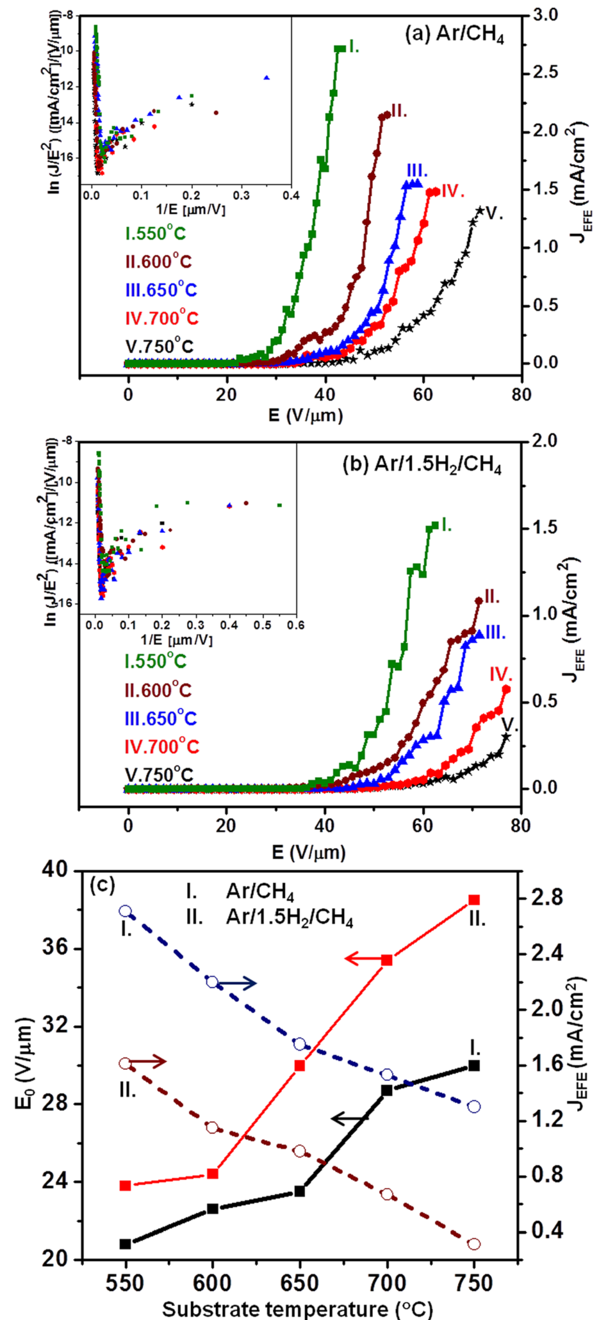

FIG. 4. T_S dependence of electron field emission properties of UNCD films deposited in (a) Ar/CH_4 plasma, (b) $Ar/1.5\%\ H_2/CH_4$ plasma, and (c) the variation of turn-on field (E_0) and EFE current density (J_{EFE}) with the substrate temperature used for growing the films.

the working pressure and d is the cathode-to-anode distance. The γ-value is then calculated from the minimum breakdown voltage $(V_{bk})_{min}$ of each Paschen curve using Eq. (2). The Paschen curves of the two series of UNCD films are shown in Figs. 7(a) and 7(b), revealing that the V_{bk} is lowest at around "pd" = 19.99 Pa cm. The $(V_{bk})_{min}$ value changes systematically with the T_S (Fig. 8(a)) and the smallest value is achieved for the $UNCD_{550Ar}$ films (curve I, Fig. 8(a)). By knowing the $(V_{bk})_{min}$ and the corresponding "pd" values, the γ values of the two series of UNCD films were calculated from Eq. (2). The γ-coefficients thus obtained are shown in Fig. 8(b) and are summarized in Table II, indicating that the γ-value varies moderately due to the increase in T_S or the addition of 1.5% H_2 in Ar/CH_4 plasma. However, the $UNCD_{550Ar}$ films show slightly higher γ-value (0.2604) than the other UNCD films (0.2503–0.2591).

It should be mentioned that the $(E_{th})_{PI}$ required to trigger the Ar plasma for the microplasma devices using diamond as cathodes is perceptibly smaller than the $(E_0)_{EFE}$ for inducing the EFE process. Although the $UNCD_{550Ar}$ films possess much lower E_0 (20.8 V/μm) for the EFE process as compared with that of the other UNCD films (22.6–38.5 V/μm, cf. Table I), the E_{th} for triggering the illumination process does not show much difference when the cathode material is

[This article is copyrighted as indicated in the article. Reuse of AIP content is subject to the terms at: http://scitation.aip.org/termsconditions. Downloaded to] IP: 163.13.36.187 On: Mon, 27 Oct 2014 02:41:45

TABLE I. Electron field emission properties of UNCD films grown at various substrate temperatures using Ar/CH_4 and $Ar/1.5\%\ H_2/CH_4$ plasma.

	$UNCD_{Ar}$ Ar/CH_4 (99/1)		$UNCD_{1.5H}$ $Ar/H_2/CH_4$ (97.5/1.5/1)	
Temperature (°C)	E_0 (V/μm)	J_{EFE} (mA/cm^2) @ 50.0 (V/μm)	E_0 (V/μm)	J_{EFE} (mA/cm^2) @ 65.0 (V/μm)
550	20.8	$\geq$2.71	23.8	$\geq$1.61
600	22.6	2.20	24.4	1.15
650	23.5	1.75	30.0	0.98
700	28.7	1.53	35.4	0.67
750	30.0	$\leq$1.30	38.5	$\leq$0.31

changed from the $UNCD_{550Ar}$ to $UNCD_{nAr}$ (or $UNCD_{nH}$) films ($(E_{th})_{550Ar} = 0.21$ V/μm to $(E_{th})_{nAr,nH} = 0.22$–0.24 V/μm). Such a phenomenon is due to the difference in the mechanism for igniting plasma in an Ar environment and that for turning on the EFE process in a high vacuum environment (10^{-6} Torr (1.3×10^{-4} Pa)). In a microplasma device, the plasma can be triggered when the electrons emitted from the cathode (secondary electrons) gain sufficient kinetic energy to ionize the gas molecules (e.g., 15.7 eV for Ar species). The ionization cross-section for Ar species increases with kinetic energy of the electrons and reaches a maximum value at around 100 eV.[40] Before the onset of plasma, the electric field imposed on the cathode materials is far below the E_0 needed for inducing the EFE process. Only the secondary electrons contribute to trigger the ionization of Ar gas molecules for inducing the onset of plasma illumination. Therefore, it seems that the low EFE E_0 for the $UNCD_{550Ar}$ films is not helpful in lowering the threshold field for igniting the plasma. However, when the plasma is ignited, a plasma sheath is formed in the vicinity of cathode, where the electric field will be markedly increased. For typical plasma with a sheath around 10 μm in thickness, the electric field

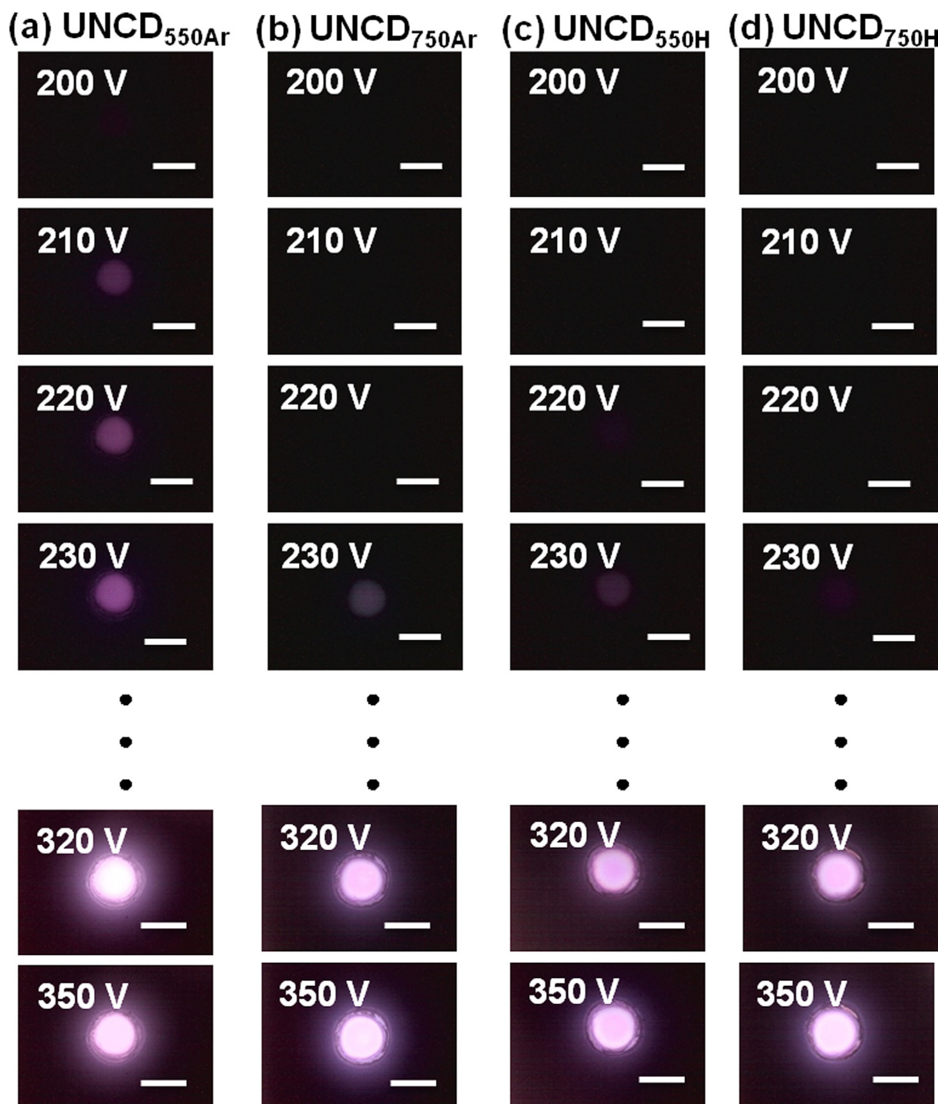

FIG. 5. Plasma illumination characteristics for the microplasma devices utilizing (a) $UNCD_{550Ar}$, (b) $UNCD_{750Ar}$, (c) $UNCD_{550H}$, and (d) $UNCD_{750H}$ as cathodes (the scale length in all the figures represents 5 mm).

[This article is copyrighted as indicated in the article. Reuse of AIP content is subject to the terms at: http://scitation.aip.org/termsconditions. Downloaded to] IP: 163.13.36.187 On: Mon, 27 Oct 2014 02:41:45

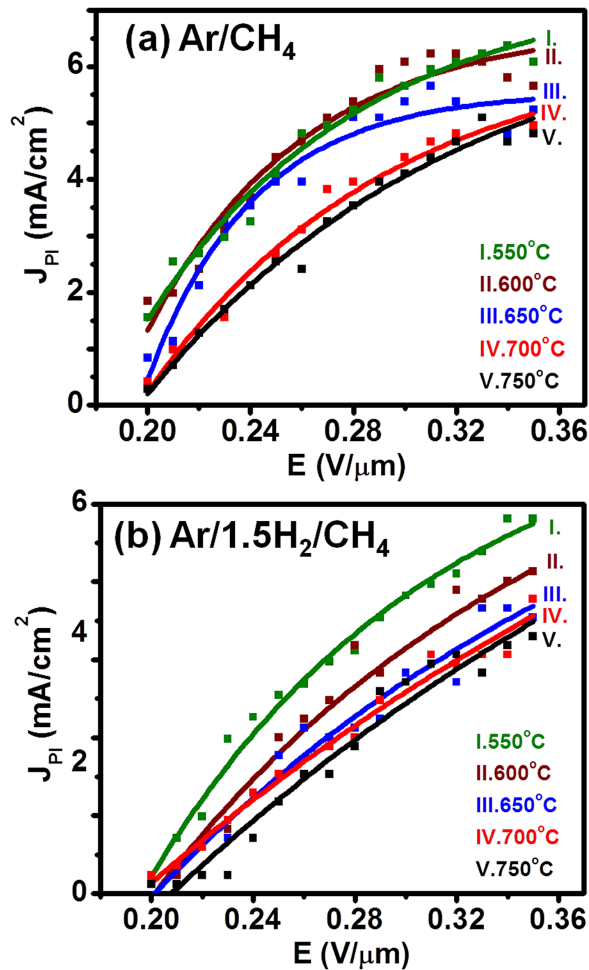

FIG. 6. T_S dependence of plasma illumination properties of UNCD films deposited in (a) Ar/CH_4 plasma and (b) Ar/1.5% H_2/CH_4 plasma.

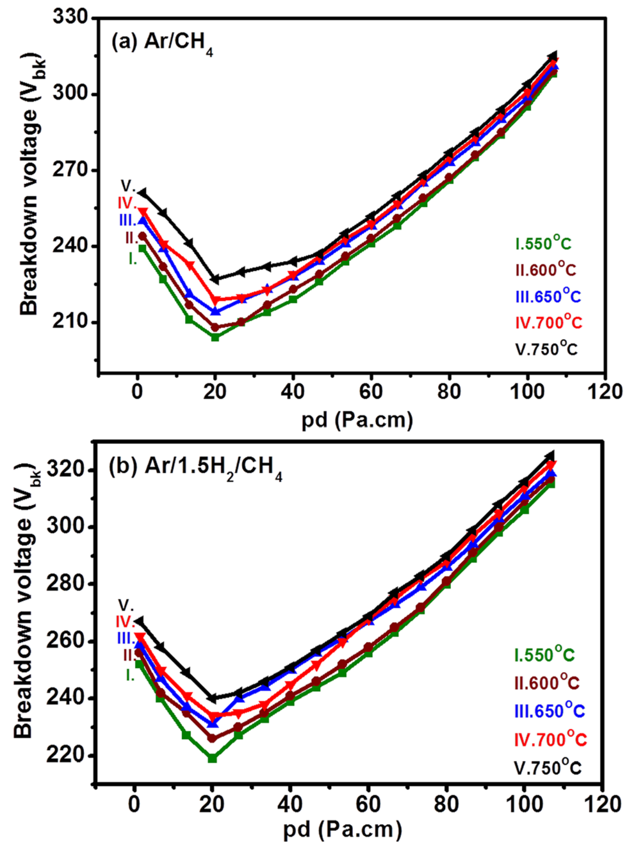

FIG. 7. T_s dependence of Paschen curves of UNCD films deposited in (a) Ar/CH_4 plasma and (b) Ar/1.5% H_2/CH_4 plasma.

experienced by the cathode will increase to around 35.0 V/μm corresponding to an applied voltage of 350 V. Such a field is far larger than necessary for turning on the EFE process for most of the diamond films. A large number of electrons will be emitted from the diamond cathode materials that then increase the cascading ionization for the Ar gas molecules and increase markedly J_{PI}. Therefore, a larger J_{PI} is observed when the $UNCD_{550Ar}$ films are used as cathodes, i.e., $(J_{PI}) = 4.38\,mA/cm^2$, as they emit more EFE current density.

The better PI characteristics of $UNCD_{550Ar}$ films are intimately correlated with their superior EFE properties. But the question arising now is what is/are the genuine factor(s) enhancing the EFE and PI properties of $UNCD_{550Ar}$ films? To understand the mechanism that alters the EFE as well as PI properties of the films deposited in Ar/CH_4 and Ar/1.5% H_2/CH_4 plasma at different T_S, a TEM microstructural investigation is needed to verify the changes of the hybridized carbon phase in the films. A TEM image of $UNCD_{550Ar}$ (Fig. 9(a)) along with the selective area electron diffraction (SAED) pattern (inset, Fig. 9(a)) shows that the clusters in the film consist of a random distribution of spherical UNCD grains of 5–7 nm in diameter with distinct structured grain boundaries. A detailed examination of the SAED pattern reveals that beside the commonly observed (111), (220), and (311) diffraction rings corresponding to c-diamond of Fd3m symmetry, there are extra diffraction rings, which correspond to n-diamond, the fcc structure of the diamond phase. Figure 9(b) shows a high-resolution TEM (HRTEM) image corresponding to Fig. 9(a) for $UNCD_{550Ar}$ films. This figure reveals that $UNCD_{550Ar}$ is composed of grains ~5 nm in size. The image b_1 (marked as region b_1 in Fig. 9(b)) is the

TABLE II. Plasma illumination properties of UNCD films grown at various substrate temperatures using Ar/CH_4 and Ar/1.5% H_2/CH_4 plasma.

	$UNCD_{Ar}$ Ar/CH_4 (99/1)			$UNCD_{1.5H}$ Ar /H_2/CH_4 (97.5/1.5/1)		
Temperature (°C)	E_{th} (V/μm)	J_{PI} (mA/cm^2) @ 0.25 (V/μm)	γ-coefficient	E_{th} (V/μm)	J_{PI} (mA/cm^2) @ 0.25 (V/μm)	γ-coefficient
550	0.21	4.38	0.2604	0.23	2.54	0.2558
600	0.21	4.10	0.2591	0.23	2.40	0.2538
650	0.22	3.96	0.2572	0.24	2.12	0.2525
700	0.22	2.68	0.2555	0.24	1.84	0.2517
750	0.23	2.54	0.2535	0.24	1.41	0.2503

[This article is copyrighted as indicated in the article. Reuse of AIP content is subject to the terms at: http://scitation.aip.org/termsconditions. Downloaded to] IP: 163.13.36.187 On: Mon, 27 Oct 2014 02:41:45

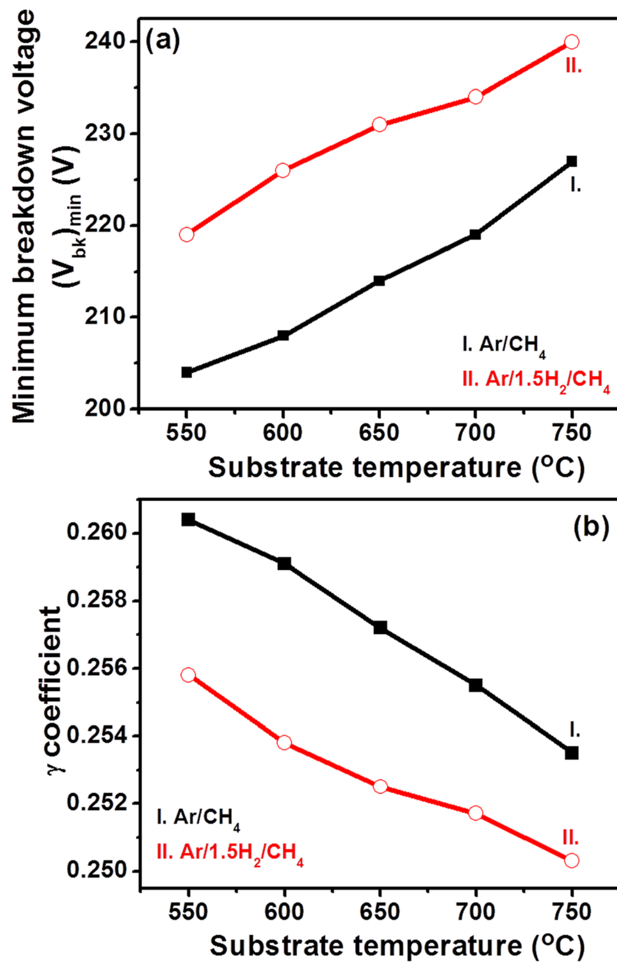

FIG. 8. T_S dependence of (a) minimum breakdown voltage $(V_{bk})_{min}$ and (b) γ-coefficient values of UNCD films deposited in (I) Ar/CH_4 plasma and (II) $Ar/1.5\% H_2/CH_4$ plasma.

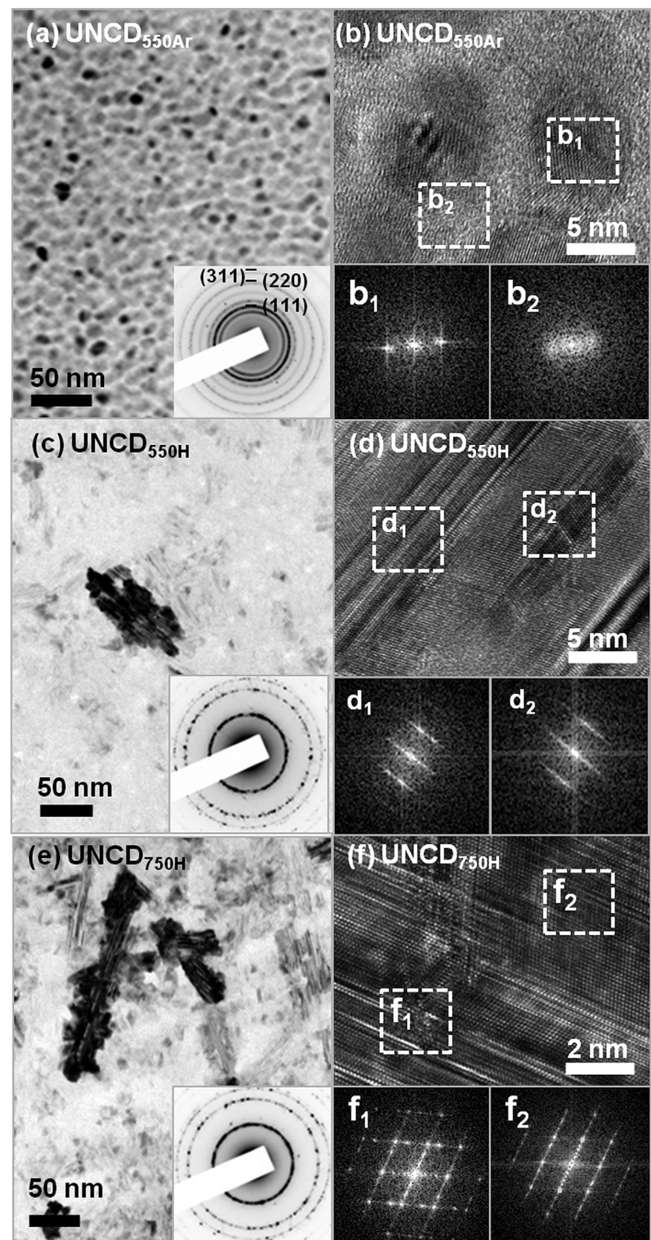

FIG. 9. Bright field TEM images of (a) $UNCD_{550Ar}$, (c) $UNCD_{550H}$, and (e) $UNCD_{750H}$, with the insets showing the corresponding SAED patterns of each image. HRTEM image of (b) $UNCD_{550Ar}$, (d) $UNCD_{550H}$, and (f) $UNCD_{750H}$ (figures in the insets show the FT diffractogram of different regions in these UNCD films).

Fourier-transformed (FT) diffractogram corresponding to the diamond phase, whereas b_2 (marked as region b_2 in Fig. 9(b)) corresponds to the sp^2-bonded *a-C* phase. Restated, the $UNCD_{550Ar}$ films contain a larger proportion of sp^2-bonded *a-C* phase along the grain boundaries.

In the TEM image of $UNCD_{550H}$ (Fig. 9(c)), the grains are shown to agglomerate, forming large elongated clusters of a few hundred nanometers in size. The spotty and ring patterns in the SAED image (inset, Fig. 9(c)) arise from the large diamond aggregates with randomly oriented diamond grains in the film. It should be noted that the dark image of the agglomerate observed in Fig. 9(c) is the diamond clusters oriented along some zone axis, strongly diffracting the electron beams. The surrounding regions also contain large diamond agglomerates, but they are oriented away from the zone axis and thus weakly diffracting the electron beams, showing no contrast. Unlike that observed for the $UNCD_{550Ar}$ films, no extra diffraction ring, besides the (111), (220), and (311) diamond rings, is detected in this SAED pattern. The diamond aggregates in $UNCD_{550H}$ films are presumably formed by coalescence of the ultra-small diamond grains that lead to a lesser proportion of grain boundaries as compared with the $UNCD_{550Ar}$ films. The detailed microstructure of the agglomerates in $UNCD_{550H}$ films is best demonstrated by a structure image, which is shown in Fig. 9(d). Large diamond aggregates, which are formed due to the addition of 1.5% H_2 in Ar/CH_4 plasma, contain complicated defect structures. The FT images numbered d_1 and d_2 in Fig. 9(d) are of the regions numbered similarly in the HRTEM images, showing evidence of diamond polytypes, which are mostly of hexagonal structure (designated as *n*H).

The TEM image of $UNCD_{750H}$ (Fig. 9(e)) also shows large cluster formation (60–180 nm) with grain boundaries almost diminished. The large clusters of grains oriented in different directions overlap one another, forming a dendrite geometry. The increase in T_S gives rise to a more marked coalescence process, resulting in a larger size of clusters, endorsing a complicated structure with a higher proportion

[This article is copyrighted as indicated in the article. Reuse of AIP content is subject to the terms at: http://scitation.aip.org/termsconditions. Downloaded to] IP: 163.13.36.187 On: Mon, 27 Oct 2014 02:41:45

of defects in these clusters, as observed in the HRTEM image of $UNCD_{750H}$ (Fig. 9(f)). The micrograph clearly gives evidence of polymorphs of diamond and the presence of stacking faults and hexagonal diamond plates observed as the crisscrossed streaks in the images. The corresponding FT images (f_1 and f_2) (marked square regions f_1 and f_2 in Fig. 9(f)) show the stacking faults as well as the polytypes of *n*H type diamonds. As a consequence of large cluster formation, the concentration of planar defects is larger, while the proportion of grain boundaries is lower, for $UNCD_{750H}$ in comparison with that of $UNCD_{550H}$. The $UNCD_{750Ar}$ films (figure not shown) possess similar microstructure as that shown in Figs. 9(c) and 9(d) implying that the increase in T_S has the same effect as the addition of 1.5% H_2 in Ar/CH_4 plasma in inducing the coalescence of nanosized diamond grains. The TEM investigation provides more information on the evolution of microstructure of UNCD films when T_S was increased or 1.5% of H_2 was added into the Ar/CH_4 plasma, viz. the grain size increases and grain boundaries decrease, which are consistent with the previous analyses of Raman and NEXAFS spectra.

The above-described results have clearly illustrated the influence of T_S and 1.5% H_2 in Ar/CH_4 plasma on inducing such changes on morphological, structural, and bonding characteristics of UNCD films synthesized by a MPECVD system. To explore the growth mechanism possibly involved, the information regarding the constituents of the plasma bombarding the substrate, the OES of the Ar/CH_4 plasma and Ar/1.5 H_2/CH_4 plasma, were recorded *in situ* (Fig. 10). The Ar/CH_4 plasma (Fig. 10(a)) is predominated with the Swan band near 468.0, 516.0, and 563.0 nm,[41] which are mainly the emissions from the C_2 species and CH species observed at $\sim$386.0 nm. A small spectral line from the atomic hydrogen species, H_α (656.3 nm)[42,43] was observed only for Ar/1.5% H_2/CH_4 plasma (Fig. 10(b)). The OES spectra for both series of UNCD films at different T_S remain the same. The C_2 dimer is initially thought to be the one important player in the grain growth mechanism for UNCD films grown in Ar/CH_4 plasma.[44] But recent reports showed that apart from the C_2 dimers, the competition between H atoms, CH_3 radicals, and other C_1 species reacting with dangling bonds on the surface determine the renucleation behavior and thereby the morphology of the diamond films.[45–47] Although the mechanisms of the grain growth in UNCD films are still not well understood, it is clear that films grown at low T_S (550 °C) in Ar/CH_4 plasma possess ultra-nano diamond grains with spherical or random geometry and have a uniform size distribution with well defined grain boundaries of considerable thickness.[41] Apparently, the clear grain boundary phase, no matter whether it is pure carbon with disorderly bonded suggested by Gruen *et al.*[48] or hydrocarbons (e.g., *t*-PA) suggested by Ferrari,[49] is formed only at low T_S in Ar/CH_4 plasma. The mechanism, which forms uniformly nano-sized grains, is believed that the CH species adhere to the diamond clusters forming an encapsulating layer of *t*-PA phase that prevents the C_2 (or other active carbon species) to attach to the existing diamond clusters. The C_2 (or other active carbon species) can only renucleate new diamond clusters, resulting in ultra-small grains granular structure for $UNCD_{550Ar}$ films that are schematically illustrated in the inset of Fig. 10(a).

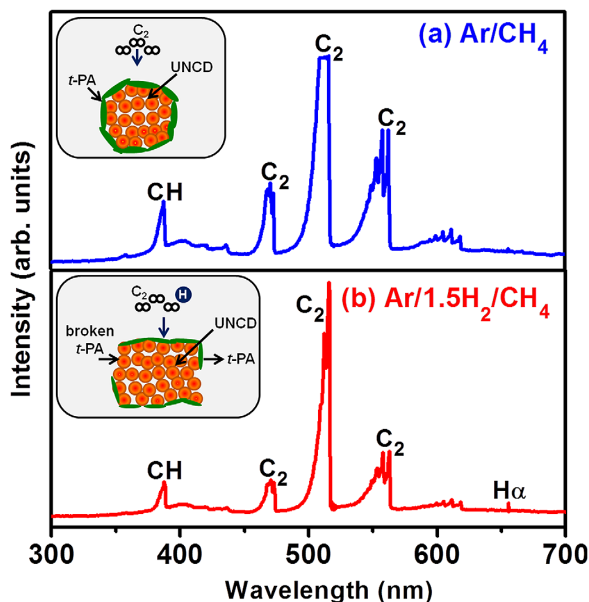

FIG. 10. Typical optical emission spectra of (a) Ar/CH_4 plasma (inset shows the schematic grain growth mechanism of films deposited in Ar/CH_4 at $T_S = 550$ °C) and (b) Ar/1.5% H_2/CH_4 plasma used for growing UNCD films (inset shows the schematic grain growth mechanism of films deposited in Ar/1.5% H_2/CH_4 plasma).

The addition of 1.5% H_2 in Ar/CH_4 reactant gas content induces the presence of high content of atomic hydrogen in the plasma. During the initial stages of grain growth, the CH species occupy the surface of nano-sized diamond clusters, while the CH bonding later form into *t*-PA chains.[50,51] In the meantime, the incoming excess hydrogen breaks the *t*-PA bonds by prompting diffusion of existent H in the CH bonds.[52] Such breaking and diffusion of H may not be clearly evident in the film deposition in Ar/CH_4 plasma because of the generation of H which may be just ample enough for the CH bond formation without causing excessive bond breaking. Hence, the excess atomic hydrogen bombardment may be the cause of extensive breaking of the *t*-PA bonds thereby leading to preferential etching of hydrocarbons attached to diamond surfaces.[41,53] This would allow the C_2 (or active carbon) in the plasma to further attach to these surfaces, leading to anisotropic growth of the grains, as observed from SEM and TEM images of films grown in $Ar/H_2/CH_4$ plasma.[41] Such a process is schematically shown in the inset of Fig. 10(b).

In spite of such reports on the grain growth of films deposited in different plasma, the importance of T_S in defining the origin of grain boundary phases and thereby influence the EFE properties of the films has not been highlighted. At $T_S > 550$ °C, *t*-PA attaches scarcely to diamond clusters because high T_S can destroy the *t*-PA chains in the grain boundaries, causing desorption of the hydrogen from the sample. The lack of *t*-PA at the grain boundaries would mean lesser net efficiency of CH to adhere to diamond and uneven passivation of the diamond phase by the *t*-PA chains and thereby anisotropic grain growth.

From the grain growth model, it is clear that C_2 (or other active carbon) species in Ar/CH_4 plasma are responsible for

[This article is copyrighted as indicated in the article. Reuse of AIP content is subject to the terms at: http://scitation.aip.org/termsconditions. Downloaded to] IP: 163.13.36.187 On: Mon, 27 Oct 2014 02:41:45

the growth of diamond grains and that CH species passivate the UNCD grains only at the low T_S, leading to a large fraction of non-diamond phase in the grain boundaries of $UNCD_{550Ar}$ films. The grain boundary conduction mechanism allows electrons to be emitted easily through them. The $UNCD_{550Ar}$ films possess more emission sites that then lead to superior EFE properties, viz. low E_0 and high J_{EFE} values (curve I, Fig. 4(a)). Our argument is well supported by the model proposed by Cleri *et al.*[54] in which the hopping conduction through localized π^* states in sp^2-bonded grain boundaries represents a viable mechanism for transporting electrons to the film surface. Moreover, the low E_0 of $UNCD_{550Ar}$ films can emit the electrons at lower voltages, which can participate in ionizing the Ar gas molecules of PI studies. As a result there will be a significant variation in plasma current density, which follows the same trend as the E_0 of EFE behavior. But UNCD films other than $UNCD_{550Ar}$ have large clustered grains with a lesser number of grain boundaries possessing a hindrance for the electrons to emit from the surface resulting in poor emission sites and hence inferior EFE properties. As a result, the presence of non-diamond phases in the grain boundaries of UNCD films is a genuine factor for the superior EFE and PI properties.

IV. CONCLUSIONS

UNCD films are grown by MPECVD in gas mixtures of Ar/CH_4 and $Ar/1.5\%\ H_2/CH_4$ at T_S varying from 550 to 750 °C. The changes in the sp^2 and sp^3 carbon phases in the films due to the change in plasma content and T_S are studied in detail by analyzing Raman and NEXAFS spectra. TEM investigations reveal that, at low T_S (550 °C), UNCD films grown using Ar/CH_4 plasma consist of ultra-nano diamond grains with well-defined grain boundaries. This is due to the large proportion of CH radicals, in conjunction with the C_2 radicals, which passivates the diamond clusters and enhances the nucleation of new diamond clusters. At high T_S (750 °C), the adhering efficiency of CH radicals to diamond lattice drops resulting in nanosized diamond grains that are no longer passivated; larger diamond clusters of a few tens of nanometers in size were formed, resulting in the reduction of grain boundaries. On the contrary, even at lower T_S, the introduction of H_2 in Ar/CH_4 plasma leads to more diamond cluster formation and grain boundary reduction than that observed in the $UNCD_{nAr}$ film. This is due to the weak C-H bonds that cannot passivate the diamond clusters due to desorption of hydrogen from the surface. With an increase in T_S (750 °C) in $UNCD_{nH}$, the passivation of the diamond phase is suppressed and the growth of elongated clustered grains with diminished grain boundaries is promoted. This is again due to further desorption of hydrogen from the C-H bonds at elevated T_S. Such a model on the modification on the granular structure can explain the change in the EFE and PI properties of UNCD films due to the increase in T_S and the addition of excess H_2 in the Ar/CH_4 plasma. Particularly, the $UNCD_{550Ar}$ film shows better EFE properties, viz. low E_0 of 20.8 V/μm with high J_{EFE} ($\geq$2.72 mA/cm^2 at an applied field of 50.0 V/μm) compared with other UNCD films. The existence of grain boundaries of considerable thickness ($\sim$1 nm) surrounding the ultra-nano diamond grains enhances the EFE properties of $UNCD_{550Ar}$ film. The variations of PI properties strongly correlated with the EFE properties of the UNCD films, which are found to be sensitive to changes in the microstructure of UNCD films. Investigations based on the PI properties of UNCD films support their potential use in a broad spectrum of applications in microplasma display technologies.

ACKNOWLEDGMENTS

This work was supported by the Taiwan National Science Council under Grant Nos. NSC 101-2112-M-032-002-MY2 and NSC 101-2221-E-007-064-MY3.

[1] J. G. Eden, S. J. Park, N. P. Ostrom, S. T. McCain, C. J. Wagner, B. A. Vojak, J. Chen, C. Liu, P. von Allmen, F. Zenhausern, D. J. Sadler, C. Jensen, D. L. Wilcox, and J. J. Ewing, J. Phys. D: Appl. Phys. **36**, 2869 (2003).
[2] S. J. Park, J. Chen, C. J. Wagner, N. P. Ostrom, C. Liu, and J. G. Eden, IEEE J. Sel. Top. Quantum Electron. **8**, 387 (2002).
[3] J. G. Eden, S. J. Park, N. P. Ostrom, and K. F. Chen, J. Phys. D: Appl. Phys. **38**, 1644 (2005).
[4] K. H. Becker, K. H. Schoenbach, and J. G. Eden, J. Phys. D: Appl. Phys. **39**, R55 (2006).
[5] L. G. Meng, C. L. Liu, H. F. Liang, and Z. H. Liang, Phys. Lett. A **372**, 6504 (2008).
[6] S. H. Awad and H. C. Qian, Wear **260**, 215 (2006).
[7] Z. S. Yang, H. Shirai, T. Kobayashi, and Y. Hasegawa, Thin Solid Films **515**, 4153 (2007).
[8] S. Kanazawa, R. Daidai, S. Akamine, and T. Ohkubo, Surf. Coat. Technol. **202**, 5275 (2008).
[9] R. Guchardi and P. C. Hauser, J. Chromatogr. A **1033**, 333 (2004).
[10] Y. Hozumi, T. Seto, M. Hirasawa, M. Tsuji, and A. Okuyama, J. Electrost. **67**, 1 (2009).
[11] A. Michels, S. Tombrink, W. Vautz, M. Miclea, and J. Franzke, Spectrochim. Acta B **62**, 1208 (2007).
[12] G. Auday, Ph. Guillot, and J. Galy, J. Appl. Phys. **88**, 4871 (2000).
[13] L. S. Pan and D. R. Kania, *Diamond: Electronic Properties and Applications* (Klumer Academic, Boston, 1995).
[14] P. K. Bachmann, V. van Elsbergen, D. U. Wiechert, G. Zhong, and J. Robertson, Diamond Relat. Mater. **10**, 809 (2001).
[15] K. Chakrabarti, R. Chakrabarrti, K. K. Chattopadhyay, S. Chaudhrui, and A. K. Pal, Diamond Relat. Mater. **7**, 845 (1998).
[16] T. D. Corrigan, D. M. Gruen, A. R. Krauss, P. Zapol, and R. P. H. Chang, Diamond Relat. Mater. **11**, 43 (2002).
[17] H. C. Chen, C. S. Wang, I. N. Lin, and H. F. Cheng, Diamond Relat. Mater. **20**, 368 (2011).
[18] T. G. McCauley, D. M. Gruen, and A. R. Krauss, Appl. Phys. Lett. **73**, 1646 (1998).
[19] D. M. Gruen, C. D. Zuiker, A. R. Krauss, and X. Pan, J. Vac. Sci. Technol. A **13**, 1628 (1995).
[20] W. H. Liao, C. R. Lin, and D. H. Wei, Appl. Surf. Sci. **270**, 324 (2013).
[21] K. Panda, N. Kumar, K. J. Sankaran, B. K. Panigrahi, S. Dash, H. C. Chen, I. N. Lin, N. H. Tai, A. K. Tyagi, Surf. Coat. Technol. **207**, 535 (2012).
[22] K. J. Sankaran, N. Kumar, J. Kurian, R. Ramadoss, H. C. Chen, A. K. Tyagi, S. Dash, C. Y. Lee, N. H. Tai, and I. N. Lin, ACS Appl. Mater. Interfaces **5**, 3614 (2013).
[23] H. F. Cheng, C. C. Horng, H. Y. Chiang, H. C. Chen, and I. N. Lin, J. Phys. Chem. C **115**, 13894 (2011).
[24] K. Y. Teng, P. C. Huang, W. C. Shih, and I. N. Lin, Diamond Relat. Mater. **24**, 188 (2012).
[25] R. H. Fowler and L. Nordheim, Proc. R. Soc. London, Ser. A **119**, 173 (1928).
[26] N. St. and J. Braithwaite, Plasma Sources Sci. Technol. **9**, 517 (2000).
[27] D. Mariotti, J. A. McLaughlin, and P. Maguire, Plasma Sources Sci. Technol. **13**, 207 (2004).
[28] A. C. Ferrari and J. Robertson, Phys. Rev. B **61**, 14095 (2000).
[29] S. Prawer and R. J. Nemanich, Philos. Trans. R. Soc. London, Ser. A **362**, 2537 (2004).

[This article is copyrighted as indicated in the article. Reuse of AIP content is subject to the terms at: http://scitation.aip.org/termsconditions. Downloaded to] IP: 163.13.36.187 On: Mon, 27 Oct 2014 02:41:45

[30]J. Birrell, J. E. Gerbi, O. Auciello, J. M. Gibson, J. Johnson, and J. A. Carlisle, Diamond Relat. Mater. **14**, 86 (2005).
[31]X. Xiao, J. Birrell, J. E. Gerbi, O. Auciello, and J. A. Carlisle, J. Appl. Phys. **96**, 2232 (2004).
[32]K. J. Sankaran, J. Kurian, H. C. Chen, C. L. Dong, C. Y. Lee, N. H. Tai, and I. N. Lin, J. Phys. D: Appl. Phys. **45**, 365303 (2012).
[33]J. Birrell, J. E. Gerbi, O. Auciello, J. M. Gibson, D. M. Gruen, and J. A. Carlisle, J. Appl. Phys. **93**, 5606 (2003).
[34]Y. K. Chang, H. H. Hsieh, W. F. Pong, M. H. Tsai, F. Z. Chien, P. K. Tseng, L. C. Chen, T. Y. Wang, K. H. Chen, J. R. Bhusari, J. R. Yang, and S. T. Lin, Phys. Rev. Lett. **82**, 5377 (1999).
[35]P. T. Joseph, N. H. Tai, C. H. Chen, H. Niu, H. F. Cheng, W. F. Pong, and I. N. Lin, J. Phys. D: Appl. Phys. **42**, 105403 (2009).
[36]J. Nithianandam, J. C. Rife, and H. Windischmann, Appl. Phys. Lett. **60**, 135 (1992).
[37]A. Gutierrez, M. F. Lopez, I. Garcia, and A. Vazquez, J. Vac. Sci. Technol. A **15**, 294 (1997).
[38]S. S. Chen, H. C. Chen, W. C. Wang, C. Y. Lee, I. N. Lin, J. Guo, and C. L. Chang, J. Appl. Phys. **113**, 113704 (2013).
[39]L. Ponsonnet, C. Donnet, K. Varlot, J. M. Martin, A. Grill, and V. Patel, Thin Solid Films **319**, 97 (1998).
[40]A. Bogaerts, M. Yan, R. Gijbels, and W. Goedheer, J. Appl. Phys. **86**, 2990 (1999).
[41]C. S. Wang, H. C. Chen, H. F. Cheng, and I. N. Lin, J. Appl. Phys. **107**, 034304 (2010).
[42]J. Ma, N. Michael, R. Ashfold, and Y. A. Mankelevich, J. Appl. Phys. **105**, 043302 (2009).
[43]G. Balestrino, M. Marinelli, E. Milani, A. Paoletti, I. Pinter, A. Tebano, and P. Paroli, Appl. Phys. Lett. **62**, 879 (1993).
[44]D. Zhou, T. G. McCauley, L. C. Qin, A. R. Krauss, and D. M. Gruen, J. Appl. Phys. **83**, 540 (1998).
[45]P. W. May, Yu. A. Mankelevich, J. N. Harvey, and J. A. Smith, J. Appl. Phys. **99**, 104907 (2006).
[46]J. R. Rabeau, P. John, J. I. B. Wilson, and Y. Fan, J. Appl. Phys. **96**, 6724 (2004).
[47]P. W. May and Yu. A. Mankelevich, J. Phys. Chem. C **112**, 12432 (2008).
[48]D. M. Gruen, A. R. Krauss, C. D. Zuiker, R. Csencsits, L. J. Terminello, J. A. Carlisle, I. Jimenez, D. G. J. Sutherland, D. K. Shuh, W. Tong, and F. J. Himpsel, Appl. Phys. Lett. **68**, 1640 (1996).
[49]A. C. Ferrari and J. Robertson, Phys. Rev. B **63**, 121405 (2001).
[50]K. M. McNamara, D. H. Levy, K. K. Gleason, and C. J. Robinson, Appl. Phys. Lett. **60**, 580 (1992).
[51]Sh. Michaelson and A. Hoffman, Diamond Relat. Mater. **15**, 486 (2006).
[52]W. Yang, O. Auciello, J. E. Butler, W. Cai, J. A. Carlisle, J. E. Gerbi, D. M. Gruen, T. Knickerbocker, T. L. Lasseter, J. N. Russell, L. M. Smith, and R. J. Hamers, Nature Mater. **1**, 253 (2002).
[53]R. Pfeiffer, H. Kuzmany, P. Knoll, S. Bokova, N. Salk, and B. Gunther, Diamond Relat. Mater. **12**, 268 (2003).
[54]F. Cleri, P. Keblinski, L. Colombo, D. Wolf, and S. R. Phillpot, Europhys. Lett. **46**, 671 (1999).

[This article is copyrighted as indicated in the article. Reuse of AIP content is subject to the terms at: http://scitation.aip.org/termsconditions. Downloaded to] IP: 163.13.36.187 On: Mon, 27 Oct 2014 02:41:45